IOP Publishing | International Atomic Energy Agency Nuclear Fusion
Nucl. Fusion **54** (2014) 064001 (7pp) doi:10.1088/0029-5515/54/6/064001

Influence of the electric and magnetic shears on tokamak transport

K.C. Rosalem[1], **M. Roberto**[1] **and I.L. Caldas**[2]

[1] Departamento de Física, Instituto Tecnológico de Aeronáutica, 12228-900, São José dos Campos, SP, Brazil
[2] Instituto de Física, Universidade de São Paulo, 05315-970, São Paulo, SP, Brazil

E-mail: kaue@ita.br

Received 27 June 2013, revised 19 January 2014
Accepted for publication 13 February 2014
Published 23 May 2014

Abstract

We applied a non-integrable drift-kinetic model, valid for large aspect ratio tokamaks, to investigate plasma edge particle transport driven by drift waves. Particle transport is obtained from the chaotic trajectories obtained by numerically integrating the canonical equations of motion, for the total flow formed by the equilibrium sheared flow and few dominant resonant drift waves propagating in the sheared equilibrium magnetic field. Thus, we investigate the transport dependence on the radial profiles of the electric and magnetic fields and show that radial particle transport at the plasma edge can be reduced by properly modifying the electric and magnetic shear profiles. For non-monotonic radial electric fields, we also observe non-twist transport barriers with shearless invariants identified by extremum values of the rotation number profiles of the invariant curves. The observed non-twist barriers are modified by the magnetic shear and persist for magnetic shear variations expected in present tokamaks.

Keywords: tokamak transport, drift wave, magnetic shear, electric shear

(Some figures may appear in colour only in the online journal)

1. Introduction

The plasma confinement in tokamaks is limited by the particle transport at the plasma edge much higher than the values predicted by neoclassical transport theory by collisions in toroidal geometry [1, 2]. In this context, the influence of the electric and magnetic equilibrium fields on the particle transport induced by the plasma edge turbulence is nowadays under investigation in all tokamaks [3, 4]. Thus, it has been recognized that the interpretation of the observed anomalous particle transport has to take into account the spatial profiles and their associated shears of the electric and magnetic fields at the plasma edge.

At the plasma edge the turbulence-driven particle transport is mainly caused by the particle $\boldsymbol{E} \times \boldsymbol{B}$ drift [5–7] and the fluctuating electrostatic field is associated with drift waves, driven by equilibrium radial gradients, propagating in the poloidal direction. Several experiments show that this transport can be reduced by properly changing the electric field radial profile [8, 9]. One experimental procedure to reduce the transport is to apply an electric field bias modifying the non-uniform radial electric field and resulting sheared flow [10–12]. Moreover, electrode biasing has been applied to verify the influence of the electric shear on the plasma transport and the formation of edge transport barriers [13].

To interpret particle transport at the tokamak plasma edge, non-integrable drift models with chaotic dynamics have been proposed for large aspect ratio tokamaks [14–16]. Following this approach, a model has been proposed to describe the transport by drift waves propagating in the plasma edge of tokamaks with equilibrium $\boldsymbol{E} \times \boldsymbol{B}$ poloidal flow, for uniform magnetic fields [16, 17] and magnetic fields with shear [15, 18]. Moreover, symplectic drift wave maps in the vicinity of given radial position and safety factor have been derived from these models [15, 18] to numerically investigate the transport dependence on shear spatial profiles. Thus, for these maps, the transport reduction, caused by the combined effects of radial electric field shear and both monotonic and reversed shear magnetic q profiles, has been investigated [16, 19, 20]. However, applications of the proposed models to investigate global transport in tokamaks and the escape of particles to the walls still remain to be explored by numerical integration of the equations of motion. In this model, drift waves cause chaos and the impact of chaos on the particle transport can be estimated by integrating the particle drift trajectories. In this description, the possibility of controlling the transport by modifying the shear profile can be evaluated even without considering the wave response. Moreover, the chaotic transport is caused by internal dynamic process without any external resonant magnetic perturbation.

In this work, we consider the non-integrable drift-kinetic model introduced in [15] and the canonical equations that describe the particle transport driven by drift waves. We performed numerical simulations of particle motion by integrating the canonical equations, for the total flow formed by the equilibrium sheared flow and a few dominant resonant drift waves and the sheared equilibrium magnetic field. The chaotic particle trajectories give rise to transport. Thus, we investigate effects from electric and magnetic sheared fields on plasma particle transport through a combination of numerical simulation results and concepts from Hamiltonian dynamics theory. Our analysis is based on numerical procedures used in chaos theory to investigate and describe chaotic orbits and the creation and destruction of transport barriers. One of these procedures consists in obtaining Poincaré maps for particle drift trajectories. Moreover, the chaotic orbits are integrated for a very long time in order to obtain the transport described in the paper. We show that particle transport can be reduced by modifying the electric and magnetic field profiles and that transport barrier can be displaced by properly modifying the magnetic shear at the plasma edge. As expected, the analysed topologies are typical of two-dimensional quasi-integrable Hamiltonian systems, for both twist and non-twist maps. These topologies contain several characteristics important for the particle transport and plasma confinement.

Our results can be applied to any tokamak, described in a large aspect ratio approximation, for which electric bias has been applied to control plasma transport. Even so, to show how the topology, described by shear profiles, modifies the particle transport, numerical simulations are presented for parameters taken from the Brazilian tokamak TCABR [17, 21]. However, the paper presents a conceptual investigation rather than detailed comparisons with experiments performed in any tokamak. Accordingly, the shear profiles and the drift wave spectrum are chosen to allow assessing if the induced drift wave transport is affected by changes in the electric and magnetic shear profiles.

In section 2, we introduce the drift-kinetic model used to describe particle transport driven by drift waves. In section 3, we integrate the particle trajectories and investigate the transport considering different radial electric field profiles. In section 4, for a reversed shear electric field profile, we show that transport barriers can be modified by the magnetic shear. The combined effects of magnetic and electric shears are summarized and concluded in section 5.

2. Drift–kinetic model

The model introduces the basic equations of motion to describe particle trajectories following the magnetic field lines and the electric drift. We consider an equilibrium electrostatic potential in the radial direction and electrostatic drift waves propagating in the poloidal and toroidal directions [15]. These drift waves originate from plasma edge non-uniformities in a layer of toroidal magnetic confinement. The fluctuating electrostatic potential has been assumed as a function of the amplitude, spatial and time modes.

Here, the particle trajectories are described by the guiding-centre motion,

$$\frac{\mathrm{d}\boldsymbol{x}}{\mathrm{d}t} = v_{\parallel}\frac{\boldsymbol{B}}{B} + \frac{\boldsymbol{E}\times\boldsymbol{B}}{B^2}, \tag{1}$$

and the components of this equation can be written as

$$\frac{\mathrm{d}r}{\mathrm{d}t} = -\frac{1}{Br}\frac{\partial\tilde{\phi}}{\partial\theta}, \tag{2a}$$

$$\frac{\mathrm{d}\theta}{\mathrm{d}t} = \frac{v_{\parallel}}{r}\frac{B_{\varphi}}{B} + \frac{1}{B}\frac{\partial\tilde{\phi}}{\partial r} - \frac{E_r}{B}, \tag{2b}$$

$$\frac{\mathrm{d}\varphi}{\mathrm{d}t} = \frac{v_{\parallel}}{R}, \tag{2c}$$

where $\boldsymbol{x} = (r, \theta, \varphi)$ in local polar coordinates. The considered plasma configuration corresponds to a layer of large aspect ratio tokamak. The electric field is given by equilibrium radial field E_r plus a fluctuating component $\tilde{\boldsymbol{E}} = -\nabla\tilde{\phi}$. We assume $B \simeq B_{\varphi} \gg B_{\theta}$ and the magnetic shear in this model is introduced by the safety factor profile. Moreover, the chaotic transport is caused by internal dynamic process without any external resonant magnetic perturbation.

For the fluctuating potential we use the finite mode drift wave spectrum,

$$\tilde{\phi}(\boldsymbol{x}, t) = \sum_{m,l,n}\phi_{mln}\cos(m\theta - l\varphi - n\omega_0 t - \psi_0), \tag{3}$$

where ϕ_{mln} is the mode amplitude, ω_0 is the lowest angular frequency with substantial amplitude in the drift wave spectrum and ψ_0 is a chosen initial phase. Thus, we assume either one drift wave or a set of waves that are described by the fluctuating electrostatic potential.

As it is known that the relative fluctuation levels of plasma potential are substantial in the edge [6, 22, 23], we consider a maximum electrostatic fluctuation ϕ_{MLn} in this region. Complementarily, the drift wave spectrum is mainly chosen to allow assessing if the induced drift wave transport is affected by changes in the electric and magnetic shear profiles. Thus, in the numerical simulations we consider drift wave spectra characterized by a single spatial M/L mode and one or three harmonics n in time. The self-dynamic drift wave response is not considered in our model, i.e. the spectrum is the same for different shear profiles. Even so, this model allows investigating the simultaneous influence of magnetic and electric shears on the plasma edge chaotic transport.

For convenience, we consider action and angle variables, such as $I = (r/a)^2$ and $\psi = M\theta - L\varphi$, respectively [15]. Note here that ψ plays the role of a helical angle defined by dominant modes (coherent oscillations). Taking these assumptions into equations (2*a*)–(2*c*), we obtain

$$\frac{\mathrm{d}I}{\mathrm{d}t} = \frac{2M}{Ba^2}\sum_{M,L,n}^{N}\phi_{MLn}\sin(\psi - n\omega_0 t - \psi_0), \tag{4a}$$

$$\frac{\mathrm{d}\psi}{\mathrm{d}t} = \frac{v_{\parallel}}{Rq(I)}[M - q(I)L] - \frac{ME_r}{Ba\sqrt{I}}, \tag{4b}$$

where a is the minor plasma radius, R is the major plasma radius and $q(I)$ is the safety factor profile as a function of action variable. In the next sections, particle trajectories are integrated by a fourth Runge–Kutta numerical scheme and their intersections in Poincaré sections are shown in (I, ψ) planes. The amplitude modes are chosen as $\phi_{MLn=2} = 4.90\,\mathrm{eV}$, $\phi_{MLn=3} = 0.85\,\mathrm{eV}$ and $\phi_{MLn=4} = 0.10\,\mathrm{eV}$ (see figure 1).

The self-dynamic drift wave response is not considered in our model; it means that drift wave spectrum is kept fixed. However, this model allows investigating the simultaneous influence of magnetic and electric shears at the plasma edge.

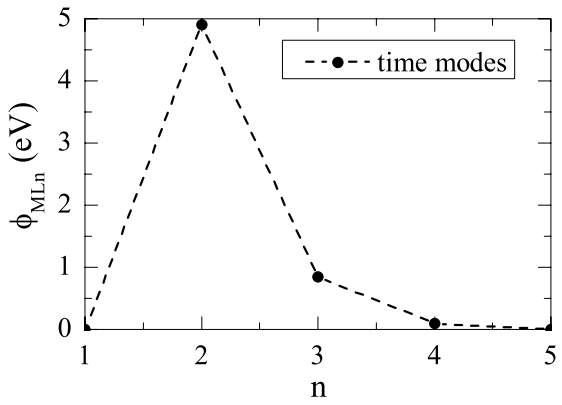

Figure 1. Drift wave spectrum for a dominant *M/L* mode and amplitudes $\phi_{MLn=2} = 4.90\,\text{eV}$, $\phi_{MLn=3} = 0.85\,\text{eV}$ and $\phi_{MLn=4} = 0.10\,\text{eV}$.

3. Electric shear effects

We assume a spatial dominant mode $M/L = 4/16$ and investigate the influence of E_r profiles by comparing different Poincaré maps and resonance conditions. The considered radial electric fields are uniform, monotonic and non-monotonic profiles, as seen in figure 2(*a*). The monotonic profiles are given by the expression $E_r = 2\alpha r + \beta$, and the non-monotonic one by $E_r = 3\alpha r^2 + 2\beta r + \gamma$, where the coefficients α, β and γ have to be defined in each case. The coefficients are set for monotonic E_r profile with positive shear as $\alpha = -1.30 \times 10^3$ and $\beta = -1.60 \times 10^3$; for monotonic E_r profile with negative shear as $\alpha = 1.30 \times 10^3$ and $\beta = -2.40 \times 10^3$; for non-monotonic E_r profile as $\alpha = -80.00 \times 10^3$, $\beta = 31.95 \times 10^3$ and $\gamma = -6.00 \times 10^3$. To these profiles correspond the electric shear profiles shown in figure 2(*b*), calculated using the equation $S_{E_r} = (r/E_r)(\mathrm{d}E_r/\mathrm{d}r)$. Thus, we assume either one drift wave or a set of waves that are described by the fluctuating electrostatic potential without considering any plasma wave response.

The simulations are performed using this set of equilibrium radial electric fields and a monotonic safety factor profile $q(r) = 1.99 + 3.99(r/a)^2$ for $r \leqslant a$, and $q(r) = q(a)(r/a)^2$ for $r > a$, with $q(a) = 5.98$ at the plasma edge. These profiles are chosen to show the influence of the magnetic shear on the drift-wave-induced transport and generate distinguishable islands to facilitate the proposed barrier and islands reconnection analyses. We consider the particle parallel velocity $v_\parallel$ constant along the particle trajectories, $v_\parallel = 2.5\,\text{km}\,\text{s}^{-1}$ [24]. The lowest angular frequency $\omega_0 = 6 \times 10^4\,\text{rad}\,\text{s}^{-1}$ has been chosen in the power spectrum obtained by floating potential measurements [21] in the TCABR tokamak. For this tokamak configuration we use $R = 61\,\text{cm}$, $a = 18\,\text{cm}$ and toroidal magnetic field $B = 1.1\,\text{T}$. Although we use TCABR parameters to show numerical examples of the transport dependence on the electric and magnetic shears, the verified dependence should be valid for any large aspect ratio tokamak for which electric bias has been applied to modify the equilibrium electric field.

In figure 3 we present the Poincaré maps by integrating equations (4*a*) and (4*b*) for various initial conditions. The solutions of this integration are selected at the toroidal section $\varphi = 2\pi/\omega_0\,\text{rad}$. In these Poincaré maps, the minor plasma radius lies at $I = 1.0$, but we show I up to 1.2 in order to identify the particle transport to the chamber wall. For the uniform E_r profile, see figure 3(*a*), chaotic particle trajectories occur for $I \gtrsim 0.6$. When changing the previous E_r profile to the monotonic one with negative shear, we observe islands almost destroyed and embedded in a chaotic sea, as can be seen in figure 3(*b*). However, periodic structures arise in $I \gtrsim 0.9$ for the monotonic E_r profile with positive shear, as seen in figure 3(*c*). Note that, the monotonic E_r shears have the same modulus but lead to distinct transport values at the plasma edge, reduced for the positive electric shear. For the non-monotonic case in figure 3(*d*), the phase space structure is deeply modified and a shearless invariant curve (depicted in blue) appears at the plasma edge. This curve is seen as a particle transport barrier that allows trapping chaotic trajectories inside the plasma. Moreover, all Poincaré maps have been obtained for the same drift wave spectrum, hence transport reduction is observed without a necessary change in the fluctuation levels of plasma potential.

Since the chaotic regions are quite similar for uniform electric field profile (figure 3(*a*)) and monotonic one with negative shear (figure 3(*b*)), we calculated the time dependence of the standard deviation for particle radial position,

$$\sigma^2(t) = \frac{1}{N}\sum_{v=1}^{N}(r_i(t) - r_i(0))^2, \tag{5}$$

for an ensemble of $N = 1000$ particles initially located from $I = 0.9$ to 1.0. In figure 4, the standard deviation for the monotonic E_r profile with negative shear indicates a smaller radial particle transport than in the uniform E_r case. Thus, introducing electric shear reduces the transport at the plasma edge. Note that assuming the same set of initial conditions and time integration, more intersections are observed in the chaotic region of the monotonic E_r field with negative shear (figure 3(*b*)). This occurs due to the confinement improving along the toroidal direction, such that more trajectory intersections are selected at the Poincaré section. Hence, the considered monotonic E_r profile generates a large enough shear in the $\boldsymbol{E} \times \boldsymbol{B}$ poloidal zonal flow to reduce the transport driven by drift waves, as first proposed by Biglari *et al* [25].

The periodic islands in the Poincaré maps can be explained by taking the resonance conditions. For this, we assume the time invariance of the action variable in equation (4*a*) that implies $\mathrm{d}/\mathrm{d}t(\psi - n\omega_0 t) \cong 0$. Then, the resonance condition is obtained when $(\mathrm{d}\psi/\mathrm{d}t)/\omega_0$ assumes values of the time mode n for a determined action I in equation (4*b*).

For the set of radial electric field profiles we calculated the resonance conditions, as shown in figure 5. This shows that the resonance $n = 4$ is related to the lowest non-zero electrostatic amplitude in the drift wave spectrum (see figure 1) and occurs at $I \cong 0.4$ for all E_r profiles. For uniform and both monotonic E_r profiles, the resonance $n = 3$ is observed as a single perturbation at $I \cong 0.8$. However, the non-monotonic case reveals the resonance $n = 3$ with double location at $I \cong 0.6$ and $I \cong 1.0$, which corresponds to the twin islands separated by invariant surfaces in figure 3(*d*). In addition to that, the resonance $n = 2$ is related to the highest electrostatic amplitude in the drift wave spectrum and provides secondary islands at the plasma edge.

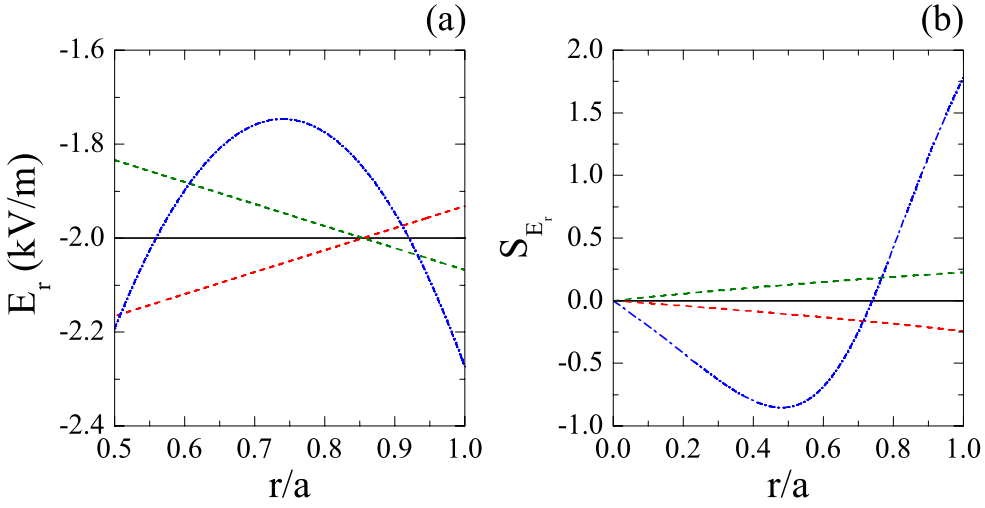

Figure 2. (*a*) Radial electric field and (*b*) electric field shear profiles for (solid black line) uniform, (dashed green/red line) monotonic with positive/negative shear and (dashed–dotted blue line) non-monotonic cases.

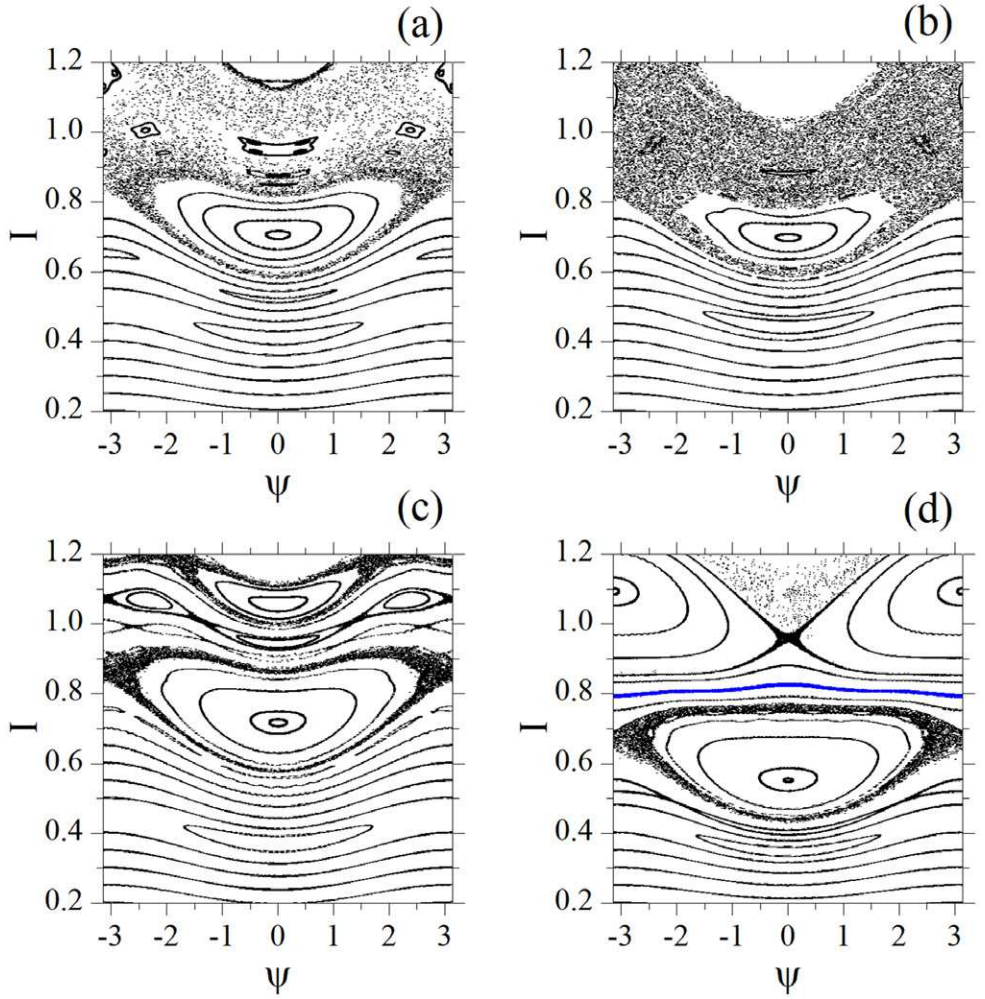

Figure 3. Poincaré maps for uniform (*a*), monotonic with negative shear (*b*), monotonic with positive shear (*c*) and non-monotonic (*d*) electric field profiles. The shearless curve is depicted in blue for the non-monotonic case.

To determine the radial position at the shearless invariant curve in figure 3(*d*), we calculate the rotation number that is defined as $\Omega = \lim_{i\to\infty} \Delta\psi_i / i$. For this, each action variable I gives an initial condition to Ω and $\mathrm{d}\Omega/\mathrm{d}I \cong 0$ leads to the shearless point shown in figure 6.

It is known that electric reversed shear may result in conditions to generate particle transport barriers located at the shearless radial position [15, 17]. In the map of figure 3(*d*) we identify such a distinctive invariant curve, in fact, a peculiar transport barrier caused by the electric reversed shear

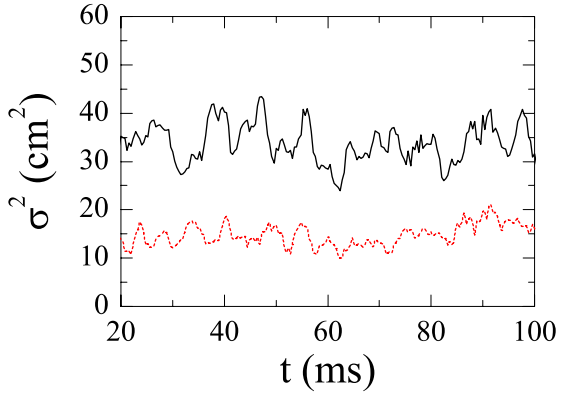

Figure 4. Standard deviation for (black line) uniform E_r profile and (dashed red line) monotonic E_r profile with negative shear.

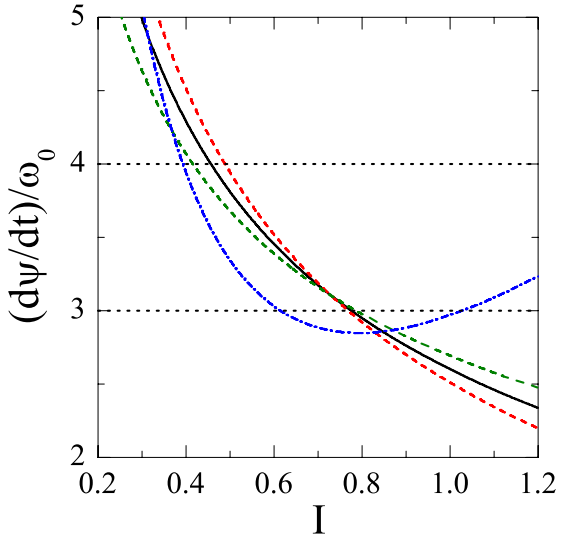

Figure 5. Resonance conditions for (solid black line) uniform, (dashed green/red line) monotonic with positive/negative shear and (dashed dotted blue line) non-monotonic E_r profiles.

configuration of figure 2, located at the shearless radial position where $d\Omega/dI \cong 0$ (see this radial position in figure 6). The indicated shearless barrier separates the particle orbits in the phase space and reduces the particle transport [26, 27]. Thus, this shearless curve acts as an internal transport barrier. Even if this barrier is broken by other waves, we expect, from other map analysis [28], that the chaotic orbits may present a large stickiness around the remaining islands, that reduces the transport. Moreover, we also observe that the magnetic shear causes a radial displacement of that barrier. Namely, note in figure 2(*b*) that the shearless position for non-monotonic E_r profile is found at $r/a \cong 0.7$, which corresponds to $I \cong 0.5$. However, the Poincaré map (figure 3(*d*)) shows the invariant curve at $I \cong 0.8$. This displacement occurs due to the magnetic shear, as can be inferred from the presence of the safety factor profile in equation (4*b*) used to calculate the phase evolution. Other magnetic shear effects on transport barriers are further analysed in more detail in the next section.

4. Magnetic shear effects

In addition to the previous section, next we further show that the magnetic shear can modify the particle orbits predicted by the

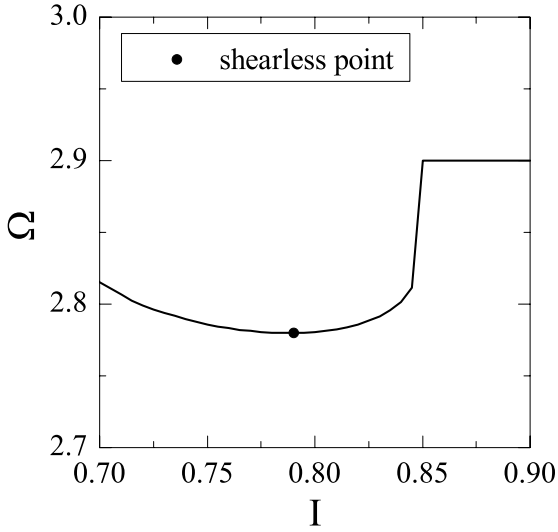

Figure 6. Rotation number profile for non-monotonic electric field case. The dot corresponds to the position of the shearless curve depicted in figure 3(*d*).

electric drift as the safety factor changes at the plasma edge. To make this effect evident we consider the non-monotonic electric shear profile of section 4 (represented by the non-monotonic dashed line of figure 2) and two different magnetic configurations, namely, two shear profiles with different $q(a)$ values. Comparing the particle orbits, represented in the Poincaré maps, we show that the alteration of the plasma edge safety factor significantly modifies the shearless transport barrier created by the considered non-monotonic electric shear profile. The described modification occurs because the less sheared magnetic configuration approaches the twin islands around the shearless transport barrier. The two safety factor profiles are chosen mainly to evidence the orbit alterations with the magnetic shear variation. These chosen profiles satisfy the resonant condition required for the existence of the shearless barrier. For example, the investigated shearless barrier does not exist for a profile varying from $q(0) = 1$ to $q(a) = 3$; although in this case the shear values are similar to those of the profile with $q(0) = 2$ and $q(a) = 4$, the necessary resonant condition is not satisfied. Yet, the attendance of the mentioned resonant condition is further evidence of the influence of the magnetic shear on the onset of transport barriers.

The magnetic shear is obtained by $S_q = (r/q)(dq/dr)$, with $q(r) = 1.99 + 1.99(r/a)^2$ for $r \leqslant a$, and $q(r) = q(a)(r/a)^2$ for $r > a$, with $q(a) = 3.98$ at the plasma edge. All the other parameters are the same as those used in the previous section.

The two safety factor and magnetic shear profiles considered in this section can be seen in figure 7. The new magnetic configuration introduced in this section, with $q(a) = 4$, has a lower magnetic shear compared with the one used in section 3 with $q(a) = 6$.

Figure 8 shows dimerized islands after a reconnection process of island separatrices [29]. This reconnection occurred due to the smaller separation between the hyperbolic point in the upper (lower) chain and the elliptic point in the lower (upper) chain caused by the magnetic shear decrease. This approach between the twin island chains can be understood

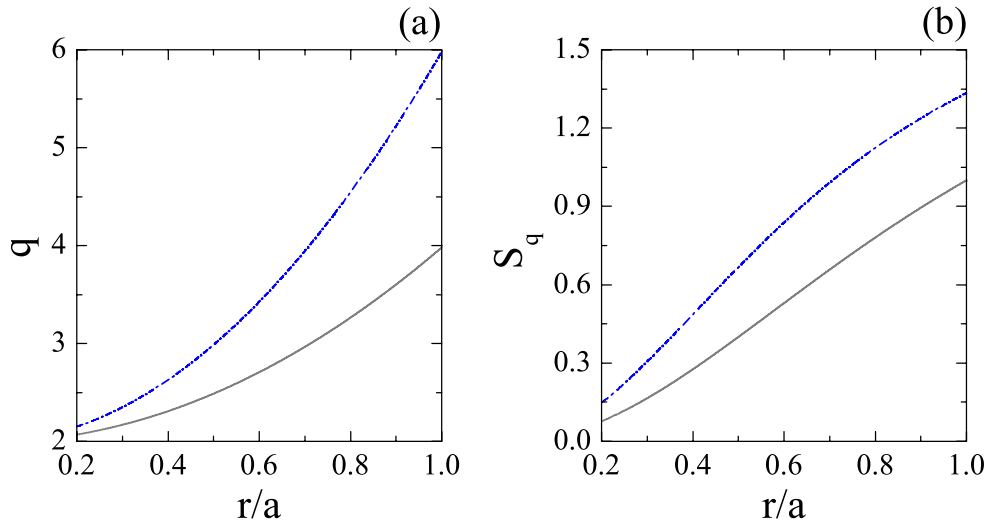

Figure 7. (a) Safety factor and (b) magnetic shear profiles for (dashed dotted blue line) $q(a) = 6$ and (solid grey line) $q(a) = 4$ cases.

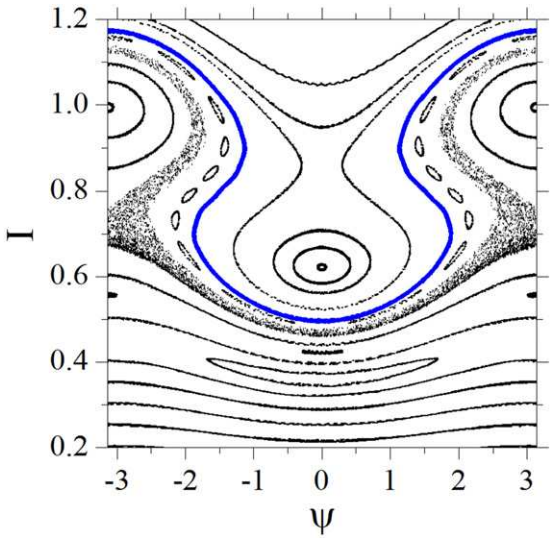

Figure 8. Poincaré maps for safety factor profile $q(a) = 4$ at the plasma edge. The shearless curve is depicted in blue.

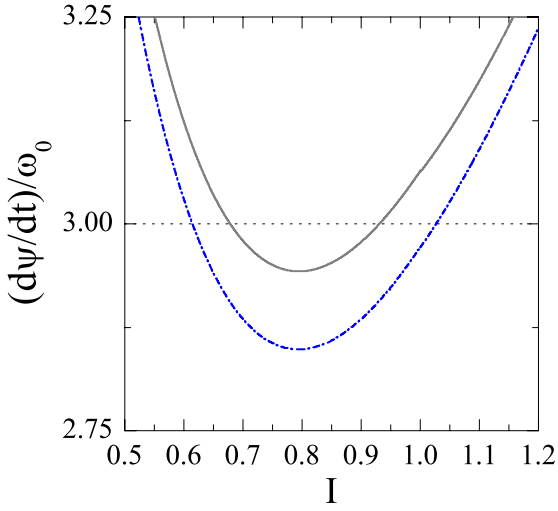

Figure 9. Resonance conditions around $n = 3$ for (dashed–dotted blue line) $q(a) = 6$ and (solid grey line) $q(a) = 4$ cases.

by verifying, in figure 9, the lower separation of the two resonance localizations (where the island chains appear) for the lower shear case. In figure 9, the resonance localization is indicated by the condition $(d\psi/dt)/\omega_0 = n = 3$. The topological difference between the twin islands around the shearless invariant curve, observed in the maps of figures 3(d) and 8, is associated with orbit reconnection. This difference is a kind of reconnection typical of non-monotonic systems that present non-twist maps with shearless curves. In addition to the island reconnection, the reduction in magnetic shear also induces the onset of meanders, robust invariant curves on both sides of the shearless curve. The reconnection and the meanders are common to the non-twist maps as described in [26, 27].

5. Conclusions

We investigated the influence of electric and magnetic equilibrium profiles on the plasma edge particle transport in tokamaks. To do so, we applied a non-integrable drift-kinetic model to describe particle transport driven by drift waves in large aspect ratio tokamaks. In this model the particle transport is due to the Lagrangian chaotic trajectories of the test particles. We performed numerical simulations of particle motion by integrating the canonical equations, for the total flow formed by the equilibrium sheared flow and a few dominant resonant drift waves and the sheared equilibrium magnetic field. Thus, we considered different radial electric field profiles and our results concerning the particle transport contained the combined effects of magnetic and electric shears. Consequently, we studied the transport dependence on the radial profiles of the electric and magnetic fields. In our numerical simulations we considered electric shear profiles representative of those observed in tokamaks with an electric bias. Rather than comparing our results with particular experiments, we looked for conceptual transport alterations expected from the profile modifications created by the biasing.

In our analysis we obtained Poincaré mappings from numerically integrated particle trajectories and compared the

extension of chaotic regions for uniform and monotonic electric and magnetic field profiles with different shears. Moreover, we also calculated the radial transport for these different profiles. Thus, we showed that particle transport at the plasma edge can be reduced by properly modifying the electric and magnetic shear profiles.

For non-monotonic radial electric field profile, we also observed non-twist transport barriers displaced from the shearless point due to the presence of the magnetic shear. The shearless curve in the Poincaré maps were identified by the extreme values of the rotation number profiles of the invariant curves. These barriers are robust and persist for magnetic shear variations expected in present tokamaks.

Acknowledgments

The authors acknowledge financial support from São Paulo Research Foundation (FAPESP, Brazil) under Grant No 2013/03401-6 and No 2011/19296-1, CNPq (Brazil), and CAPES (Brazil).

References

[1] Terry P.W. 2000 *Rev. Mod. Phys.* **72** 109
[2] Horton W. 1999 *Rev. Mod. Phys.* **71** 735
[3] Park H.-B., Heo E.-G., Horton W. and Choi D.-I. 1997 *Phys. Plasmas* **4** 3273
[4] Horton W. 2012 *Turbulent Transport in Magnetized Plasmas* (Singapore: World Scientific)
[5] Ritz C.P., Bengtson R.D., Levinson S.J. and Powers E.J. 1984 *Phys. Fluids* **27** 2956
[6] Ritz C.P. *et al* 1989 *Phys. Rev. Lett.* **62** 1844
[7] Ritz C.P., Lin H., Rhodes T.L. and Wootton A.J. 1990 *Phys. Rev. Lett.* **65** 2543
[8] Oost G.V. *et al* 2003 *Plasma Phys. Control. Fusion* **45** 621
[9] Hidalgo C., Pedrosa M.A. and Gonçalves B. 2002 *New J. Phys.* **4** 51
[10] Devynck P., Stckel J., Admek J., Ďuran I., Hron M. and Oost G.V. 2003 *Czech. J. Phys.* **53** 853
[11] Weynants R.R. 2001 *J. Plasma Fusion Res. Ser.* **4** 3
[12] Oost G.V., Gunn J.P., Melnikov A., Stöckel J. and Tendler M. 2001 *Czech. J. Phys.* **51** 957
[13] Wagner F. 2007 *Plasma Phys. Control. Fusion* **49** 1
[14] Miskane F., Garbet X., Dezairi A. and Saifaoui D. 2000 *Phys. Plasmas* **7** 4197
[15] Horton W., Park H.-B., Kwon J.-M., Strozzi D., Morrison P.J. and Choi D.-I. 1998 *Phys. Plasmas* **5** 3910
[16] Horton W. 1985 *Plasma Phys. Control. Fusion* **27** 937
[17] Marcus F.A., Caldas I.L., Guimarães-Filho Z.O., Morrison P.J., Horton W., Kuznetsov Y.K. and Nascimento I.C. 2008 *Phys. Plasmas* **15** 112304
[18] Kwon J.-M., Horton W., Zhu P., Morrison P.J., Park H.-B. and Choi D.-I. 2000 *Phys. Plasmas* **7** 1169
[19] Mouden M.El., Saifaoui D., Dezairi A., Zine B. and Eddahby M. 2007 *J. Plasmas Phys.* **73** 439
[20] Imzi H., Saifaoui D., Dezairi A., Miskane F. and Benharraf M. 2002 *Eur. Phys. J. Appl. Phys.* **17** 45
[21] Nascimento I.C. *et al* 2005 *Nucl. Fusion* **45** 796
[22] Marcus F.A., Kroetz T., Roberto M., Caldas I.L., da Silva E.C., Viana R.L. and Guimarães-Filho Z.O. 2008 *Nucl. Fusion* **48** 024018
[23] Ferreira A.A., Heller M.V.A.P. and Caldas I.L. 2000 *Phys. Plasmas* **7** 3567
[24] Severo J.H.F., Nascimento I.C., Tsypin V.S. and Galvão R.M.O. 2003 *Nucl. Fusion* **43** 1047
[25] Biglari H., Diamond P.H. and Terry P.W. 1990 *Phys. Fluids* B **2** 1
[26] Caldas I.L., Viana R.L., Szezech J.D. Jr, Portela J.S.E., Fonseca J., Roberto M., Martins C.G.L. and da Silva E.J. 2012 *Commun. Nonlinear Sci. Numer. Simul.* **17** 2021
[27] del Castillo-Negrete D. and Morrison P.J. 1993 *Phys. Fluids* A **5** 948
[28] Szezech J.D. Jr, Caldas I.L., Lopes S.R., Viana R.L. and Morrison P.J. 2009 *Chaos* **19** 043108
[29] Roberto M., da Silva E.C., Caldas I.L. and Viana R.L. 2004 *Phys. Plasmas* **11** 214